Conservative antiphase boundary in $SrTiO_3$ films on $LaAlO_3$ substrates with $SrRuO_3$ buffer layers

J. S. Wu,[a] C. L. Jia, and K. Urban
Institut für Festkörperforschung, Forschungzentrum Jülich, GmbH, D-52425 Jülich, Germany

J. H. Hao and X. X. Xi
Department of Physics, The Pennsylvania State University, University Park, Pennsylvania 16802

(Received 21 November 2000; accepted for publication 23 February 2001)

We have studied the microstructure of $SrTiO_3$ films on $LaAlO_3$ substrates with the $SrRuO_3$ buffer layer using high-resolution transmission electron microscopy. While high density of defects due to lattice mismatch were found at the $SrRuO_3/LaAlO_3$ interface, no misfit dislocation was observed at the $SrTiO_3/SrRuO_3$ interface. The {111} stacking fault in the $SrRuO_3$ buffer layer propagates into the $SrTiO_3$ film, giving rise to a type of antiphase boundary on the {110} plane with a crystallographic shear vector of $a/2\langle 001\rangle$. The boundary is a conservative one which does not lead to any charge defects. A model based on dislocation interactions is proposed to explain the generation mechanism of the antiphase boundary. © *2001 American Institute of Physics.*
[DOI: 10.1063/1.1367881]

I. INTRODUCTION

It is known that $SrTiO_3$ is an interesting dielectric material and suitable in various applications such as voltage tunable filters, oscillators, and phase shifters for microwave circuits. However, the properties of $SrTiO_3$ thin films, which are necessary for device applications, often deviate from the bulk values.[1,2] In this connection, it has been found that the atomic structure can deviate substantially from that observed in bulk materials. In $SrTiO_3$ thin films, a columnar structure has been reported as the dominant structural characteristic.[1–4] The columnar subgrain boundaries were found to be associated with misfit dislocations at the film/substrate interface in epitaxial $SrTiO_3$ films on $LaAlO_3$ substrates.[4] Recently, employing $SrRuO_3$ as the buffer layer, high-quality $SrTiO_3$ films with near single-crystal level dielectric loss were successfully prepared on $LaAlO_3$ substrates.[5]

In this article, we report on a detailed structural analysis of these films, in which a type of conservative antiphase boundary was observed. A high density of planar defects in the $SrRuO_3/LaAlO_3$ interface was found in agreement with earlier observations in single-layer $SrRuO_3$ films on $LaAlO_3$ substrates.[6] Instead of perfect misfit dislocations, stacking faults bounding partial dislocations were found to play an important role in misfit accommodation. However, in the $SrTiO_3/SrRuO_3$ interface we hardly find any misfit dislocations since the misfit between $SrTiO_3$ and $SrRuO_3$ is small. According to the lattice parameters of their pseudocubic-perovskite unit cells at room temperature, the misfit between $SrRuO_3$ and $LaAlO_3$ is 3.6%, while that for the $SrTiO_3/SrRuO_3$ system is only 0.64%. The antiphase boundaries identified in $SrTiO_3$ layer are the results of planar defects in the $SrRuO_3$ layer which run across the interface into the $SrTiO_3$ device layers.

II. EXPERIMENT

The bilayer $SrTiO_3/SrRuO_3$ films were grown by pulsed laser deposition on single crystal $LaAlO_3$ substrates. Details of the growth procedure are given in the literature.[5,7] Cross-sectional samples were prepared by cutting films along the (100) and (110) planes of $LaAlO_3$ (referring to the pseudocubic-perovskite unit cell). Two slices were glued face to face and then embedded in epoxy resin. After the glue had been cured, disks with a diameter of 3 mm were obtained by cutting away redundant epoxy. These disks were then ground, dimpled and polished, followed by Ar-ion milling in a stage cooled with liquid nitrogen. High-resolution transmission electron microscopy (HRTEM) investigations were carried out in a JEOL 4000EX electron microscope operated at 400 kV. HRTEM image simulations were carried out using the Mac-Tempas software.[8]

III. RESULTS AND DISCUSSION

Figure 1 shows a cross-sectional image at low magnification of a two-layer $SrTiO_3/SrRuO_3$ film on $LaAlO_3$ taken along the [110] axis (in this article, we will refer to their pseudocubic-perovskite unit cells). The lower $SrRuO_3$ layer exhibits two {111} planar defects. They run into the interface at positions marked by two arrows labeled 1 and 2. At these locations faults originate which run into the $SrTiO_3$ layer. The fault at arrow 1 does not show any contrast due to a relatively high specimen thickness. Close inspection of the fault at arrow 2, in an area of lower specimen thickness, shows that the fault can shift its habit plane stepwise in the [110] direction.

Figure 2 shows the area indicated by arrow 2 in Fig. 1 at a high magnification. A (111) stacking fault in the $SrRuO_3$

[a]Present address: Department of Physics and Astronomy, Arizona State University, Tempe, AZ 85287; electronic mail: jinsong.wu@asu.edu

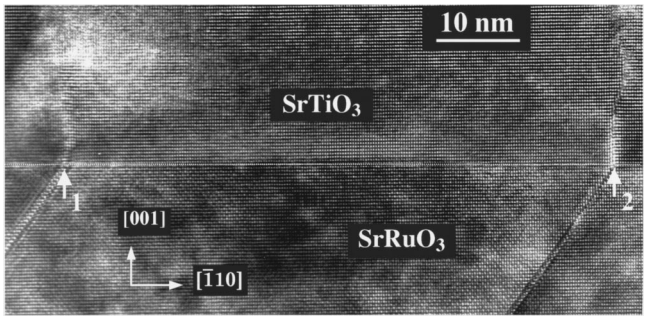

FIG. 1. A cross-sectional HRTEM image at low magnification of a $SrTiO_3$ film on $LaAlO_3$ substrate with $SrRuO_3$ as buffer layer, taken along the [110] direction. Columnar grain boundaries are associated with {111} planar defects in the $SrRuO_3$ layer.

layer (lower part of the image) propagates upward until it reaches the $SrTiO_3/SrRuO_3$ interface. As a consequence, an antiphase boundary is introduced in the $SrTiO_3$ crystal. Apart from these two types of planar defects, the cubic-to-cubic epitaxial relationship is perfectly developed. The stacking fault in the $SrRuO_3$ layer can be determined as an extrinsic one with an extra plane inserted between two (111) lattice planes. We use a Burgers circuit exhibiting three closure failures to identify the Burgers vector of the dislocation at the junction of the stacking fault and the antiphase boundary. As shown in Fig. 2, the first one is a projected displacement vector crossing the stacking fault a1. The second is a projected displacement vector crossing the antiphase boundary a2, while the third is an additional displacement vector a3. Thus, the projected Burgers vector of the dislocation can be calculated as: $\boldsymbol{b}_{\text{proj}} = \text{a1} + \text{a2} + \text{a3} = a/3[\bar{1}\bar{1}4] + a/2[\bar{1}\bar{1}2] = a/6[\bar{2}21]$.

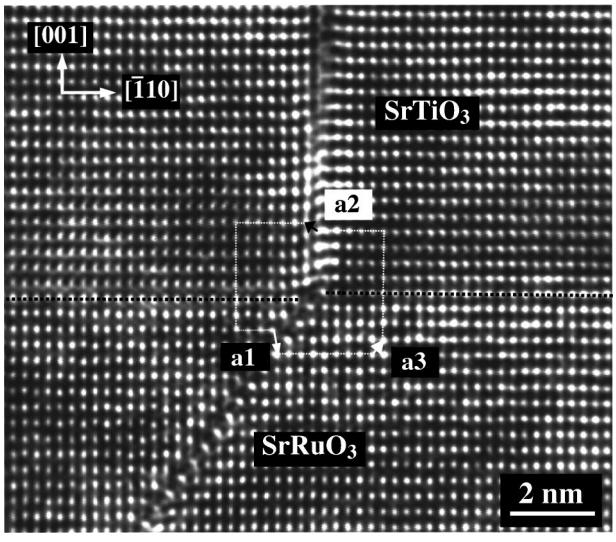

FIG. 2. Cross-sectional image of the area around arrow 2 of Fig. 1 at high magnification. A staking fault in the $SrRuO_3$ layer propagates upward to the $SrTiO_3/SrRuO_3$ interface and introduces an antiphase boundary in the $SrTiO_3$ layer. A Burgers cicruit consisting of three parts of closure failures is drawn to determine the Burgers vector of the dislocation at the junction of the stacking fault and the antiphase boundary. A black dotted line marks the $SrTiO_3/SrRuO_3$ interface.

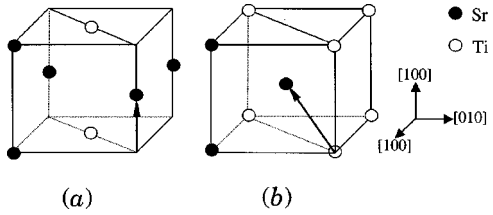

FIG. 3. Two atomic structural models of the antiphase boundaries in the (110) plane, with a crystallographic shear vector $\boldsymbol{R} = a/2[001]$ (a) and $\boldsymbol{R} = a/2[\bar{1}\bar{1}\bar{1}]$ (b).

In general, antiphase boundaries are characterized by a crystallographic shear vector $\boldsymbol{R}$ describing the relative displacement of the two parts of the crystal on either side of the interface. In Fig. 2, the antiphase boundary in the $SrTiO_3$ layer is in the (110) plane although the stacking fault in the $SrRuO_3$ layer is in the (111) plane. For the crystallographic shear vector of the antiphase boundary there are two possibilities, according to Fig. 2. The first type is $\boldsymbol{R} = a/2[001]$, as shown in Fig. 3(a), while the second type has $\boldsymbol{R} = a/2[\bar{1}\bar{1}\bar{1}]$ in Fig. 3(b). The shear vector can only be identified if the same type of defect is studied along another direction, e.g., [100].

Figure 4 shows a cross-sectional image of the $SrTiO_3/SrRuO_3$ interface taken along the [100] direction. Stacking faults in the $SrRuO_3$ layer and antiphase boundaries in $SrTiO_3$ cannot be seen directly in this orientation since they are not in an edge-on condition along this direction. However, possible displacement components along the [010] and [001] directions could still be recognized if such components occur. According to the structural models in Fig. 3, in the projection along the [100] direction there is an area where the two parts separated by the antiphase boundary overlap. Thus, the boundary appears extended in the figure.

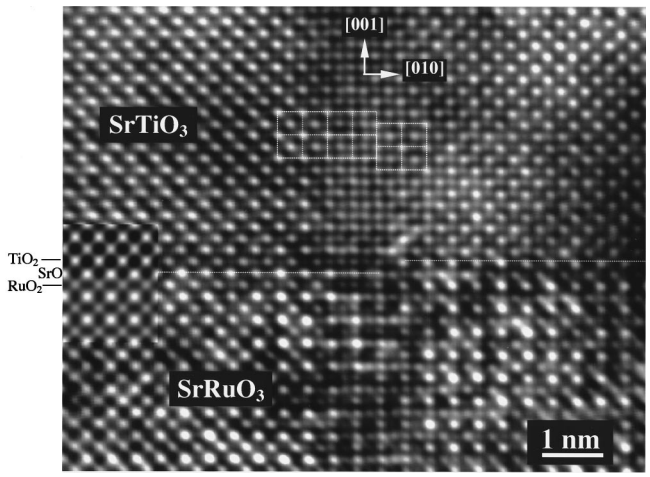

FIG. 4. Cross-sectional image taken along the [100] direction. In the middle, an antiphase boundary grows into $SrTiO_3$ crystal from $SrRuO_3$ layer. A simulated image of $SrTiO_3/SrRuO_3$ interface for a defocus value of -68 nm and a sample thickness of 5.2 nm is patched in. In the simulated image the relatively bright dots represent the position of Sr atoms in $SrRuO_3$ crystal. Cubic perovskite unit cells formed by connecting the dots reprsenting Sr atoms in $SrTiO_3$ crystal are related to each other by a projected shear vector $a/2[001]$ crossing the antiphase boundary. A white dotted line illustrates the $SrTiO_3/SrRuO_3$ interface.

Once again, the cubic-to-cubic orientation relationship is well established in the left-hand and right-hand parts separated by the planar defects, respectively. In order to distinguish the Sr and Ti positions in the $SrTiO_3$ crystal, we construct an atomic structural model of the $SrTiO_3/SrRuO_3$ interface with the atomic layer sequence of $\cdots(SrO)(RuO_2)/(SrO)(TiO_2)\cdots$. The simulated image (defocus value -68 nm and sample thickness 5.2 nm) which best matched the experimental one was inserted in the left-hand part of Fig. 4, where the atomic planes are also indicated. In the $SrRuO_3$ layer part of the image, the relatively bright dots correspond to the Sr atomic positions. In the $SrTiO_3$ layer part under the same calculating conditions, however, there is no pronounced difference in image contrast between the Sr and Ti atomic positions, which is consistent with the experimental observation. Connecting those dots representing Sr atoms to form the perovskite cubic unit cells as shown by white rectangles, it is found that they are related to each other by a shear of $a/2[001]$ crossing the antiphase boundary. In other words, no displacement along the [010] axis is found. Thus, the crystallographic shear vector $\boldsymbol{R}$ is determined as $a/2[001]$ which is constant with the atomic structural model in Fig. 3(a).

We note that the antiphase boundary is in the $(\bar{1}10)$ plane and the displacement vector $\boldsymbol{R}$ is $a/2[001]$. This is different from the well-known ''Ruddlesden–Popper'' planar defects with a crystallographic shear of $a/2\langle 111\rangle$ in the $\{100\}$ planes in Sr-rich $(SrO)(SrTiO_3)_n$ phases, where n is the number of perovskite layers separating the defects.[9,10] Since $\boldsymbol{R}\cdot\boldsymbol{n}=0$ where $\boldsymbol{n}$ is the normal vector of the boundary plane, the antiphase boundary is a conservative one. It implies that this type of antiphase boundary does not change the local composition nor does it generate any charged defects. This may provide an explanation for the observation that our $SrTiO_3$ films on the $SrRuO_3$ buffer layers showed physical properties similar to those of a single crystal. It has been reported that deviations from the ideal stoichiometric composition, with special regard to the O and Sr contents, were detrimental for the properties of $SrTiO_3$ films.[4]

In the following, we will discuss the formation mechanism of this type of antiphase boundary based on a model of interaction of the dislocations. In general, the crystallographic shear vector of a antiphase boundary is equal to the burgers vector of the dislocation that produces the antiphase boundary on glide. In $SrRuO_3$ crystal with perovskite structure, the $\{111\}$ stacking fault is assumed to extend driving by a gliding Shockley partial with $\boldsymbol{b}=a/3\langle 112\rangle$.[11] As shown in Fig. 2, the dislocation with projected Burgers vector in the $(1\bar{1}0)$ plane being $a/6[\bar{2}21]$ is found at the junction of the $(\bar{1}11)$ stacking fault and the $(\bar{1}10)$ antiphase boundary. Since the vector $a/6[\bar{2}21]$ is in the (110) plane, its projection on the plane yields the same result. Considering the possible reactions between dislocations, we can derive the dislocation reaction as

$$a/3[\bar{1}12]\rightarrow a/6[\bar{2}21]+a/2[001].$$

The reaction is energetically favorable since the $|\boldsymbol{b}|3e2/a^2$ values decrease from 6/9 to 1/4+1/4=1/2. The partial with

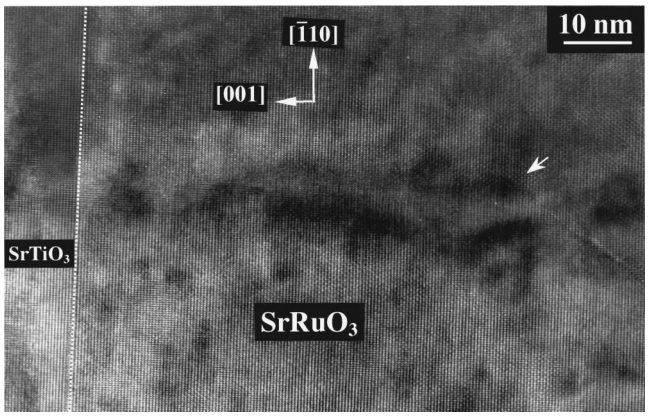

FIG. 5. A cross-sectional image taken along the [110] direction. A white arrow shows the place where a {111} planar defect transforms into the (110) antiphase boundary in $SrRuO_3$ layer. The antiphase boundary then grows into the $SrTiO_3$ layer.

$\boldsymbol{b}=a/6[\bar{2}21]$ remains at the junction to compensate for some displacement components of the Shockley partial. At the same time, the partial dislocation with $\boldsymbol{b}=a/2[001]$ glides in the $(\bar{1}10)$ plane producing a type of antiphase boundary in $SrTiO_3$. Obviously, the Burgers vector of this partial equals the crystallographic shear vector $\boldsymbol{R}$ of the antiphase boundary. In such a way, a $\{111\}$ stacking fault in $SrRuO_3$ layer transforms smoothly into a $\{110\}$ antiphase boundary in the $SrTiO_3$ layer.

The dissociation of Shockley partial dislocations also occurs in the $SrRuO_3$ layer. Figure 5 shows such a situation in Bragg diffraction contrast. Here the antiphase boundary forms in the $SrRuO_3$ layer as shown by an arrow and then propagates into the $SrTiO_3$ layer. In Fig. 4, if we draw a Burgers circuit around the region with the antiphase boundary involved in $SrTiO_3/SrRuO_3$ interface, no dislocation can be found. Thus, Fig. 4 in fact shows the same phenomenon where the antiphase boundary is formed in the $SrRuO_3$ layer and then grows directly into the $SrTiO_3$ crystal.

IV. CONCLUSIONS

In conclusion, the columnar subgrain boundary in the $SrTiO_3$ on the $SrRuO_3$ buffer is determined as a type of antiphase boundary in the (110) plane with a crystallographic shear vector $\boldsymbol{R}$ of $a/2[001]$. Composition fluctuations at the grain boundaries and charged defects harmful to the physical properties are avoided since this type of antiphase boundary is a conservative one. The partial dislocation with $\boldsymbol{b}=a/2\langle 001\rangle$ producing the antiphase boundary in the $SrTiO_3$ layer is dissociated from a Shockley partial with $\boldsymbol{b}=a/3\langle 112\rangle$ bounding a $\{111\}$ stacking fault in the $SrRuO_3$ buffer layer. This type of antiphase boundary is generated by the stacking fault in the buffer layer which can be considered as the result of ''defect epitaxy.''

ACKNOWLEDGMENTS

J. S. Wu is grateful for support from the Alexander von Humboldt-Stiftung. The work at Pennsylvania State is par-

tially supported by NSF under Grant No. DMR-9702632 and by the DARPA FAME Program under Contract No. DABT63-98-1-002.

[1] S. Yamamichi, T. Sakuma, K. Takemura, and Y. Miyasaka, Jpn. J. Appl. Phys., Part 1 **30**, 2193 (1991).
[2] H. Yamaguchi, S. Matsubara, and Y. Miyasaka, Jpn. J. Appl. Phys., Part 1 **30**, 2197 (1991).
[3] M. E. Tidjani and R. Gronsky, Appl. Phys. Lett. **58**, 765 (1991).
[4] L. Ryen *et al.*, J. Appl. Phys. **83**, 4884 (1998).
[5] H. C. Li, W. D. Si, A. D. West, and X. X. Xi, Appl. Phys. Lett. **73**, 190 (1998).
[6] P. Lu, F. Chu, Q. X. Jia, and T. E. Mitchell, J. Mater. Res. **13**, 2302 (1998).
[7] V. I. Merkulov, J. R. Fox, H. C. Li, W. D. Si, A. A. Sirenko, and X. X. Xi, Appl. Phys. Lett. **72**, 3291 (1998).
[8] R. Kilaas, *Proceedings of the 45th Annual Electron Microscopy Society of America Meeting, Baltimore, Maryland, edited by G. W. Bailey* (San Francisco, San Francisco, 1987), p. 66.
[9] S. N. Ruddlesden, and P. Popper, Acta Crystallogr. **11**, 54 (1958).
[10] R. J. D. Tilley, J. Solid State Chem. **21**, 293 (1977).
[11] O. Eibl, P. Pongratz, and P. Skalicky, Philos. Mag. B **57**, 521 (1988).